

Nonlinear effects in sputtering of organic liquids by keV ions

Iosif S. Bitensky

Departamento de Física, Pontificia Universidade Católica, C.P. 38071, Rio de Janeiro 22452-970, Brazil

Douglas F. Barofsky

Department of Agricultural Chemistry and Environmental Health Sciences Center, Oregon State University, ALS 1007, Corvallis, Oregon 97331-7301

(Received 20 January 1997)

The principal features of the spike probability model are summarized, and calculations based on the model are compared with the keV-ion sputtering data recently obtained from organic liquids. This data, which includes yields for anions of mononucleotides, cations of an organic surfactant, and hydride ions, permits the validity of the spike probability model to be examined over a wider range of both primary particles and impact energies than heretofore possible. It is demonstrated that the nonlinear sputtering effects observed when liquid organics are bombarded by atomic and multiatomic keV ions are described well when energy straggling in the transfer of primary ion energy to the target is used as a basis for calculating the probability of forming energy spikes. This spike probability model accounts for experimental yields in several cases where treatments based solely on mean stopping power are found deficient. Specifically, the model's more complete description seems to be required when, as in the case of intact molecules sputtered from condensed organic phases, spike phenomena predominate. [S0163-1829(97)03941-6]

I. INTRODUCTION

It is known that nonlinear effects occur when solids are sputtered by ions having kinetic energies in the range of 1–100 keV (keV ions). These effects are revealed as discrepancies between the ways measured sputtering yields depend on the initial kinetic properties and the stopping powers of the incident particles and the ways linear collision cascade theory predicts these dependencies.¹ Under heavy ion bombardment, sputtering yields exhibit a nonlinear dependence on energy loss,² and under cluster ion bombardment, both total sputtering yields^{3–6} and ion sputtering yields^{7,8} show nonadditive dependencies on the number of atoms in the primary cluster ions (see also the comprehensive review by Andersen⁹). The emission of ions of both large clusters^{10–13} and intact biomolecules^{14–17} from samples bombarded by keV ions is a particularly striking manifestation of nonlinear sputtering processes. In a recent investigation of nonlinear emission of molecular ions induced by clusters of gold and of organics, including fullerenes, in the keV range,¹⁸ enhancement in yield was observed to depend on a primary projectile's particle number rather than its mass. All of these phenomena stem from the rapid formation of regions of high energy density (energy spikes) near the surfaces of the targets.

When the stopping power ($\epsilon = dE/dx$) for a single, incident keV ion is high, as is the case, for example, when a heavy ion strikes a target composed primarily of heavy atoms, the probability of forming an energy spike approaches unity. In this case, the impact of the incident ion, whose mean free path is comparable with the interatomic distances in the target, can initiate numerous, overlapping cascades of elastic collisions that rapidly and efficiently impart a significant fraction of the ion's considerable kinetic energy to a small volume near the surface of the target.^{19,20} If the aver-

age energy conveyed to each atom in the spiked volume is of the order of the atomic binding energy, the region is rapidly converted into a hot gas that erupts in a single, collective event that contributes to the total sputtering yield. When such events occur, it is possible to neglect the losses due to energy straggling, i.e., fluctuations in stopping power, and to account for sputtering yield solely in terms of the mean value of ϵ . Different versions of thermal spike models^{21–23} and the shock wave model²⁴ embody such a description of nonlinear sputtering yields in instances of high ϵ for keV ions.

When ϵ is low for an incident ion, as is the case, for example, when a heavy ion impacts a target comprised of light elements, the probability of forming an energy spike is much less than unity. In such instances, occurrences of spikes are not revealed through the dependency of total sputtering yield on ϵ , which in these cases is linear, but rather through a variety of anomalous effects that conspicuously testify to the breakdown of linear transport theory.¹ Various examples have been reported. The relatively abundant secondary emission of intact biomolecular ions, containing from tens to nearly thousands of atoms, from organic targets bombarded by Cs^+ (Refs. 14–17) certainly cannot be credited to a linear phenomenon. The sputtering of ions from organic insulators by low-energy particle beams has been reviewed recently by Ens.²⁵ Comparisons of the observed sputtering yields per primary atom when Au is sputtered respectively by Xe^+ and Xe_2^+ with the same impact velocities⁶ indicate that nonlinear effects occur with the diatomic projectiles at energies well outside the range predicted by the thermal spike model. Transmission electron micrographs of gold surfaces bombarded with Bi^+ and Bi_2^+ have revealed that craters caused by only 1.5% of the Bi_2^+ (100 keV/ion) account for about 40% of all the atoms sputtered.²⁶ This observation indicates that fluctuations in the energy deposited by primary ions play an important role in nonlinear sputtering events.

Insights into the nature of nonlinear sputtering effects induced by keV ions have also resulted from computer simulations. Shapiro and Tombrello found statistically significant nonlinear yields from Cu targets for bombardment with Kr and Xe dimers but not for bombardment with Ar and Cu dimers; in the cases of Ar and Cu, however, both the energy and polar angular distributions of the sputtered atoms, which are more sensitive to nonlinear effects, exhibit features similar to those found for Kr impacts.²⁷ These results emphasize that nonlinear effects cannot be observed in the total sputtering yield when spikes are rare events. Furthermore, the outcomes of these simulations plus secondary ion yields measured by others in subsequent experiments^{7,8} suggest that nonlinear sputtering effects generated by multiatomic primary ions are more likely to be observed in the emission of multiatomic clusters than in the emission of single atoms. Computer simulations of spikes induced in condensed rare gases by keV-atom bombardment exhibited pronounced occurrences of high sputtering fluctuations.^{28,29} Most recently, Yang *et al.* concluded from the distributions of cascade defects generated in computer simulations of single ion impacts on graphite that the mean stopping power is not suitable for describing spike effects.³⁰

The examples cited in the preceding paragraphs imply that a complete theoretical description of nonlinear sputtering effects due to bombardment by keV ions should take into account the probability of energy spikes arising as significant fluctuations, i.e., straggling, in the energy losses of the primary particles. Conrad and Urbassek³¹ have, in fact, shown that fluctuations in the sputtering yield are mainly caused by fluctuations in deposited energy as conjectured earlier by Westmoreland and Sigmund.³² Probabilities of spike formation in solids have since been calculated from the distribution of energy losses that particles experience when they pass a given distance through a target.^{33,34} These computations mainly show that sputtering yield depends on the initial energy of the primary ions as well as on their stopping power and that it is necessary to consider the probability of spike formation when mean stopping power alone is insufficient to explain observed nonlinear sputtering effects. Yield curves generated from this spike probability model compare well with experimental data on biomolecules sputtered by keV-alkali ions¹⁴ and on Au sputtered by Xe₂ ions.⁶

Results from an investigation of sputtering from an organic liquid were recently reported by Yen and Barofsky.³⁵ This new body of data, which includes yields for anions of mononucleotides, cations of an organic surfactant, and hydride ions, provides an opportunity to examine the validity of the spike probability model over a wider range of both primary particles and impact energies than heretofore possible. In general, the number of secondary analyte ions ejected from the surface layer of a liquid matrix is governed by the analyte's chemical environment, its surface activity, and the dynamic properties of the impinging primary particles. Organic liquid systems fall into that sputtering regime wherein there is little likelihood of an energy spike occurring. Nonetheless, emission of intact ions of mononucleotides and organic surfactants distinctly reflects nonlinear sputtering phenomena that should be governed by the formation of spikes. Emission of the hydride ions, by contrast, indicates processes that should be governed by the formation of linear collision

cascades. Hence, this data also provides a chance to test the spike probability model against the effects of energy spikes on the emission of distinctly different classes of secondary ions.

In the present paper, pertinent features of the spike probability model^{33,34} are summarized, and calculations based on the model are compared with the keV-ion sputtering data recently obtained from organic liquids.³⁵

II. SPIKE PROBABILITY MODEL

As an energetic particle penetrates nonordered, condensed-phase matter, the energy it loses per collision along its path fluctuates due to the random nature of its encounters with the target atoms. If the magnitude of a given fluctuation in the subsurface region of the target is sufficiently large to constitute an energy spike, a nonlinear sputtering event results. In order to convert this qualitative description of nonlinear sputtering into a quantitative one, it is necessary to have (i) a criterion for the magnitude of a spike-forming energy fluctuation, (ii) an estimate of the relative likelihood of meeting this criterion, and (iii) a basis for calculating the sputtering yield from the magnitude of an energy straggling event. Each of these requirements will be considered in turn.

When a primary ion traverses a small volume of condensed phase matter, it creates an energy spike if every atom in that volume acquires sufficient energy to escape its bound state.^{19,20} Let E_{ℓ} be the energy lost by a primary particle as it passes a distance d through the target, then an energy spike will be formed if

$$E_{\ell} \geq E_c = N \eta_c \pi \bar{r}^2 d, \quad (1)$$

where N is the number of particles per unit volume of the target, η_c is a definite value of the same order as the binding energy of a target atom, and \bar{r} is the average radial extent of damage in a plane normal to the primary ion's path. Since only those spikes formed near the surface contribute to sputtering, d must be much less than the primary ion's range in the target. Therefore, angular deflection of the primary ion over this distance can be neglected.

From passage of one primary particle to the next, the magnitude of E_{ℓ} will fluctuate between 0 and E_0 , the initial kinetic energy of the primary ions. Using the expression for the probability of a monatomic ion's energy loss $f(E_{\ell}, d)$ derived by Lindhard and Nielson³⁶ and assuming that each atom of an impacting, multiatomic, primary ion passes independently through the target, Bitensky has shown that the distribution for a multiatomic projectile $f_n(E_{\ell}, d)$ is given by

$$f_n(E_{\ell}, d) = \frac{n \epsilon d \sqrt{\alpha/\pi}}{E_{\ell}^{3/2}} \exp[-\alpha(E_{\ell} - n \epsilon d)^2/E_{\ell}], \quad (2)$$

where $\alpha^{-1} = E_0[4M_1M_2/(M_1+M_2)^2]/\alpha_0 = E_0\gamma/\alpha_0$, α_0 is a numerical factor of order unity, M_1 and M_2 are the masses of a primary ion and a target atom, respectively, and n is the number of atoms in the primary ion cluster.³³ It should be noted that Lindhard and Nielson's distribution for energy loss was derived with an exponential cross section for energy transfer and $m = \frac{1}{2}$ for the Lindhard-exponent;³⁶ nevertheless, this model correctly describes energy loss due to straggling

and, as shown by Bitensky,³³ can be applied to keV-ion bombardment. Obviously from inspection of Eq. (2), the assumption of independent atomic motion becomes increasingly less tenable as n grows.

When sputtering is treated as atomic evaporation arising from a thermal spike,^{22,23} somewhat complicated nonlinear dependencies of sputtering yield on stopping power are predicted. By contrast, derivations of the sputtering yield based on the rudimentary thermal spike model²¹ and on the shock wave model²⁴ produce simple expressions containing ϵ raised to a power ($\nu=2$ and $\frac{3}{2}$, respectively). Based on this latter observation, only a general relationship between sputtering yield and stopping power, not a detailed mechanistic model, is needed to introduce the probability of spike formation into the calculation of sputtering yields. Specifically, it has been presumed³³ that this dependency has the simple form

$$Y_{\text{spike}} = \beta (E_{\ell}/d)^{\nu}, \quad (3)$$

where β is a proportionality factor that depends on the mechanisms of sputtering and ionization that produce the secondary ions, E_{ℓ}/d is the effective stopping power in the spike volume, and ν is a numerical exponent.

Taking into account the criterion for generating spikes, Eq. (1), and the probability distribution for E_{ℓ} , Eq. (2), the average spike-yield can be calculated as

$$\bar{Y}_{\text{spike}} \approx \beta \int_{E_c}^{nE_0} (E_{\ell}/d)^{\nu} f_n(E_{\ell}, d) dE_{\ell}. \quad (4)$$

Upon substituting for $f_n(E_{\ell}, d)$ and changing the integration variable to $z = E_{\ell}/n\epsilon d$, the expression for \bar{Y}_{spike} becomes

$$\bar{Y}_{\text{spike}} \approx \beta \sqrt{\frac{\alpha d}{\pi}} (n\epsilon)^{\nu+1/2} \int_{E_c/n\epsilon d}^{E_0/\epsilon d} z^{\nu-3/2} \times \exp\left[-\alpha n\epsilon d \left(z + \frac{1}{z} - 2\right)\right] dz. \quad (5)$$

Looking at Eq. (1), the lower limit of the integral, $E_c/n\epsilon d$, is easily seen to be equal to $N\eta_c(\pi\bar{r}^2/n\epsilon)$; in other words, the lower limit is inversely proportional to the energy density $n\epsilon/\pi\bar{r}^2$ created along the path of the penetrating projectile.

When primary ions suffer large energy losses, $\bar{E}_{\ell} = n\epsilon d$ is much greater than E_c , and evaluation of the integral in Eq. (5) gives

$$\bar{Y}_{\text{spike}}(\bar{E}_{\ell} \gg E_c) \approx \beta \epsilon^{\nu}, \quad (6)$$

i.e., the average sputtering yield is described solely in terms of the mean stopping power. In the opposite limit, where $\bar{E}_{\ell} = n\epsilon d$ is much less than E_c , integration yields

$$\bar{Y}_{\text{spike}}(\bar{E}_{\ell} \ll E_c) \approx \frac{\beta n \epsilon}{\sqrt{\pi(\alpha d)^{\nu-1}}} (\alpha E_c)^{\nu-3/2} e^{-\alpha E_c}. \quad (7)$$

The magnitude of this expression clearly depends on parameters, other than the stopping power, that characterize a primary ion's energy loss at the surface when the probability of forming spikes is low; however, the expression's form does not depend on the mechanism by which spikes induce sputtering in condensed phase matter. Accordingly, measured

values of yield in this limiting case are not expected to lie on a single curve when plotted against ϵ , regardless of the governing sputtering mechanism.

Actual use of Eq. (5) to compute values for the sputtering yield under a specific set of experimental conditions requires knowledge of how the average extent of damage \bar{r} from an energy spike depends on the various characteristics of both the primary ions and the target. An estimate of \bar{r} can be made by assuming it is approximately equal to the mean recoil range derived by Winterbon *et al.*³⁷ using the interaction potential $U(R) = U_0 R^{-1/m}$, i.e.,

$$\bar{r} \approx \frac{(1-m)\bar{T}^{2m}}{2mNC_1}, \quad (8)$$

where \bar{T} is the mean recoil energy, $C_1 = (\pi/2)\lambda_m a^2 (2Z_2^2 e^2/a)^m$ characterizes the recoil-recoil interaction, λ_m is a fitable numerical factor, $a = 0.8853a_0/(\sqrt{2}Z_2^{1/3})$, a_0 is the Bohr radius, Z_2 is the atomic number of the target atoms, and e is the charge of an electron. Using a differential cross section proposed by Lindhard and Nielsen,³⁶ the following expression for \bar{T} has been derived:³³

$$\bar{T} \approx \frac{\sqrt{\pi E_d/\alpha}}{2} = \frac{\sqrt{\pi E_d E_0 \gamma/\alpha_0}}{2}, \quad (9)$$

where E_d is the displacement energy of a target atom.

III. NUCLEAR STOPPING POWER

It was emphasized in the preceding sections that sputtering of atomic clusters and organic molecules by bombardment with primary ions having low, incident, kinetic energies cannot be described solely in terms of total stopping power. Nonetheless, total stopping power is an important parameter in such experiments, and for the purposes of presenting and discussing experimental data, it remains one of the most useful ones. Hence, a method for making accurate calculations of stopping power in the low-energy sputtering regime is required. In principle, both nuclear stopping and electronic stopping contribute to the total stopping power. However, the existence of an electronic stopping threshold of about 200 eV/nm has been found to exist for the ejection of biomolecules subjected to MeV ion bombardment,³⁸ and this threshold exceeds the electronic stopping powers calculated for the keV-primary ions used in the glycerol experiments³⁵ under consideration in this paper. Thus, in the case of keV-ion bombardment of organic liquids, it seems safe to assume that electronic stopping can be ignored, i.e., that $\epsilon = dE/dx = (dE/dx)_{\text{nuclear}}$.

It has been shown that the nuclear stopping power for low primary-ion energies is grossly overestimated by calculations based on the Thomas-Fermi potential but is fairly accurately represented by calculations based on interatomic potentials calculated from first principles in the free-electron approximation.³⁹ In particular, nuclear stopping power curves calculated for the Kr-C potential were found to be in excellent agreement with experimental data. Hence in this paper, the following two-parameter expression, in which $A = 0.10718$ and $B = 0.37544$ for the Kr-C potential,³⁹ has been

used for calculating reduced nuclear stopping power

$$S_{\text{nuclear}} = \frac{0.5 \ln(1 + \epsilon_0)}{\epsilon_0 + A \epsilon_0^B}, \quad (10)$$

where the reduced incident energy $\epsilon_0 = aM_2E_0/[Z_1Z_2e^2(M_1+M_2)]$, $a = 0.8853a_0/(Z_1^{1/2} + Z_2^{1/2})^{2/3}$, and Z_1 is the atomic number of the primary ion. The nuclear stopping power $(dE/dx)_{\text{nuclear}}$ has been calculated by multiplying S_{nuclear} by the factor $4\pi aNZ_1Z_2e^2M_1/(M_1+M_2)$. Nuclear stopping powers for homogeneous, multiatomic, primary ions have been approximated in this paper as the sum of the stopping powers of the primary species's constituent atoms, i.e., $\epsilon_{\text{multiatom}} = n\epsilon_{\text{atom}}$. Computer simulations of the penetration of gold clusters into silicon indicate that at low incident energies (≤ 0.1 keV/atom) a "clearing-the-way" effect dominates and that, as a consequence, the total stopping power is less than the sum of the stopping powers of the individual atoms.⁴⁰ However, this effect becomes less pronounced as incident energies increase.

IV. EXPERIMENT

The data that provides the experimental basis for this paper was obtained by bombarding liquid organic matrices with various monatomic and polyatomic metal ions having kinetic energies in the range of 7–66 keV. The apparatus and procedures used to obtain this data have been described in detail elsewhere.³⁵ Therefore, only a condensed description of the experimental system's main features are given in this article.

All measurements were made on a specially constructed, secondary ion, time-of-flight (TOF) mass spectrometer.^{41,42} Primary ion beams of Ga, In, Sn, Au, or Bi were produced in this instrument by a liquid metal ion column used in conjunction with a Wien filter. A liquid metal ion column generates a beam of singly and multiply charged ions of monatomic and polyatomic species of the metal selected for study. The Wien filter was set to allow only a homogenous subset of the metal ions exiting the liquid metal ion column, i.e., particles composed of the same number of atoms and having the same charge state, to pass through into the ion source of the mass spectrometer. This arrangement permitted the composition, energy, and momentum of the primary ion beam to be precisely defined for the secondary ion yield measurements.

The sputtering target consisted of either deoxyadenosine-5'-monophosphate (dAMP; $C_{10}H_{14}N_5O_6P$) or deoxyguanosine-5'-monophosphate (dGMP; $C_{10}H_{14}N_5O_7P$) dissolved in a solution of hexadecylpyridinium (HDP; $C_{21}H_{38}N$) acetate ($C_2H_3O_2$) and glycerol ($C_3H_8O_3$). The role of the HDP acetate, which is a surfactant, was to form ion pairs⁴³ with the anions of the dAMP or the dGMP and thereby localize the analyte on the surface of the glycerol matrix. The target solution was introduced into the ion source of the mass spectrometer as a droplet (~ 3 nL) hung on a small diameter (25 μm) tungsten wire similar to a bead on a string.

An unconventional method was employed to deliver pulses of primary ions to the target. Instead of blanking or chopping the primary beam into small, temporally and spatially bunched packets of ions, the focused primary ion beam

(~ 10 μm spot diameter) was periodically swept (1.2 kHz) across the full width of the target droplet (~ 160 μm diameter) to repeatedly sputter approximately 6 ns bursts of secondary ions off the target's surface. The dose of primary ions in a given experiment was determined from the time required to sweep the beam across the target, the number of sweeps (300 000), and the measured beam current.

Experimental estimates of absolute yields require that the transmission of the TOF analyzer and the efficiency of the detector be known accurately. Although it is difficult to obtain universal values for these two instrumental parameters, they can be maintained essentially constant over the course of a series of measurements. This makes it possible to express all the data for some fixed transmission and detection efficiency in relative terms by dividing the number of ions collected for each secondary ions species by the number of secondary ions collected for some reference species. Thus for the measurements referred to in this study, the relative yield of a given species was defined as the number of secondary ions detected in the TOF analyzer for a given dose of the primary ions used divided by the number of deprotonated dAMP ions produced by bombardment from a comparable dose of singly charged, monatomic, Au primary ions.

V. DISCUSSION

A. Evaluation of parameters

In order to make quantitative comparisons of \bar{Y}_{spike} with experimental data, it is necessary to determine the value of the exponent ν in Eq. (5). As is evident from Eqs. (6) and (7) and the discussion leading up to them, the influence of ν on \bar{Y}_{spike} depends on the nature of the sputtering conditions. With a high likelihood of forming spikes, Eq. (5) reduces to Eq. (6) in which ν plays a decisive role whereas, with a low probability of forming spikes, Eq. (5) converts to Eq. (7) in which the yield is relatively insensitive to ν . The total relative yields measured for deprotonated dAMP from the surface region of glycerol are plotted in Fig. 1 against the stopping powers of monatomic and multiatomic Bi primary ions. Bombardment with the heavy multiatomic species Bi_2^+ and Bi_3^{2+} falls within the high probability domain of spike formation, and the yields are expected therefore to depend almost entirely on stopping power. In fact, the experimental points for Bi_2^+ and Bi_3^{2+} are all fit well by a single curve, either $Y \propto \epsilon^{3/2}$ or $\bar{Y}_{\text{spike}}(\epsilon, \nu = 3/2)$ calculated with Eq. (5) for multiatomic Bi ion bombardment. For this reason, all calculations referred to in the rest of this discussion have been made with $\nu = \frac{3}{2}$.

The \bar{Y}_{spike} curves shown in the figures were generated by considering the glycerol target to be a solid consisting of atoms with $Z_2 = 3.6$ and $M_2 = 6.6u$, the mean atomic number and the mean mass respectively of glycerol ($C_3H_8O_3$), and by assigning definite values to the explicit and implicit parameters associated with Eq. (5). With the exception of β , which appears in Eq. (3), these parameters (listed in the caption of Fig. 1) have physical meaning and can be estimated to within at least an order of magnitude.

Since the magnitude of η_C , introduced in Eq. (1) as the energy necessary per atom for a spike to be formed, is of the order of the binding energy of a target atom,¹⁹ its value for

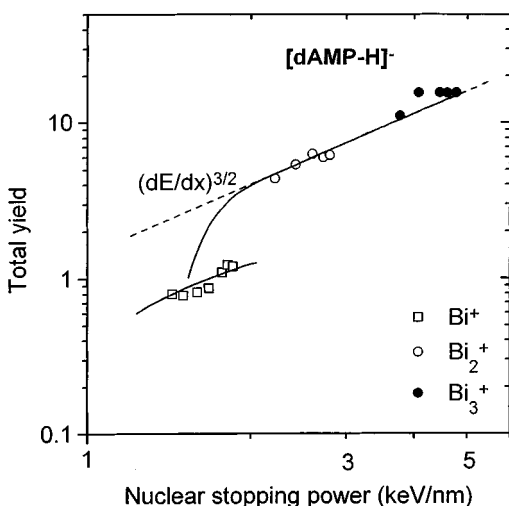


FIG. 1. Relative total yield of deprotonated dAMP molecules from the surface region of glycerol versus the stopping powers of Bi_n ions ($n=1-3$). Experimental data are from Ref. 35. Dashed line represents $Y \propto (dE/dx)^{3/2}$. Solid curves were generated with Eq. (5) by setting $\eta_c=1$ eV, $d=6$ nm, $\alpha_0=3$, $m=0.23$, $\lambda_m=0.56$, and $E_d=4$ eV.

an organic substance can reasonably be taken as the energy of a covalent bond, i.e., around 1 eV. The value 6 nm used for the parameter d , which was also introduced in Eq. (1), is approximately one third the range of a primary ion under the given experimental conditions; d is not only characteristic of the organic target but, as will be explained more fully later in this discussion, is also dependent on some of the dynamic properties of the primary particles.

The parameter α imbedded in Eq. (2) was introduced by Lindhard and Nielson into their probability distribution model³⁶ to cut off the exponential cross section for energy transfer from a projectile to a target atom at the maximum recoil energy $E_0\gamma$. Accordingly, they assumed the numerical factor α_0 to be on the order of unity. In the present instance, however, $\alpha_0=3$ yielded the best fit to the experimental data, though the results of our calculations do not vary significantly when α_0 is changed from 3 to 2.

In linear cascade collision theory, it is shown that the recoil-recoil interaction potential for cascading atoms with energies lower than a few thousand electron volts is approximated rather well by the power expression introduced in the discussion leading to Eq. (8) when $m \leq \frac{1}{3}$.³⁷ Since the average energies of the cascading atoms under consideration are on the order of hundreds of electron volts, the value 0.23 used for m in this work seems reasonable.

The fitable parameter λ_m was also introduced along with Eq. (8). Our empirical value of 0.56 is about half the theoretical λ_m value derived by Winterbon *et al.*³⁷ for $m = \frac{1}{3}$; this difference is not unreasonable when one considers that our use of Eq. (8) is in conjunction with dense collision cascades rather than the linear ones considered by Winterbon *et al.*

The displacement energy E_d found in the expression for the mean recoil energy \bar{T} , Eq. (9), enters into the theory of radiation damage in solids as the minimum recoil energy required for a stable defect to be formed. Its magnitude is usually 4–5 times larger than the binding energy of an atom

in the solid under consideration; hence in the current case, we have taken $E_d=4\eta_c=4$ eV. Since E_d comes into the calculation of \bar{Y}_{spike} through \bar{T} as $(E_d)^m$ and since $m=0.23$, the value of E_d does not significantly effect the final result (e.g., doubling E_d only increases \bar{r} by 17%).

The factor β , which includes the probabilities of a molecule being ejected as an ion and remaining intact, was obtained by fitting the theoretical curve to the single experimental point corresponding to the total relative yield of $[\text{dAMP-H}]^-$ measured at the lowest stopping power condition examined under Bi^+ bombardment. In judging how well the \bar{Y}_{spike} curves account for the experimental data, it should be borne in mind that neither the secondary ion yields described by Eq. (5) nor the measured yields used for comparison are absolute and, furthermore, that with one exception, only the single set of values for the physical parameters described in the preceding paragraph and a single value of β corresponding to one specific secondary ion were required to generate the theoretical curves. Also noteworthy in this regard is the fact that the same set of parametric values used to calculate the secondary ion yields for glycerol in this work (with the obvious exception of those for d and β) was used by Bitensky to calculate the yields of alanine ions sputtered by alkali ions from a solid film of the compound deposited on an aluminized polyester surface.³³

B. Comparison with experiment

The nonlinearity of the secondary ion yields from the surface region of glycerol can be seen more clearly in Fig. 2 where the secondary molecular ion yield per incident Bi atom is plotted versus the kinetic energy per incident Bi atom. The largest effect occurs when the primary ion is changed from Bi^+ to Bi_2^+ . The fact that the yield per atom of Bi_2^+ is about four times greater than that per atom of Bi^+ is striking considering that sputtering yield increases fairly slowly with primary ion energy and that the total kinetic energy of a Bi_2^+ projectile is only twice that of a Bi^+ projectile.

Analogous comparisons between yields measured for deprotonated dAMP under bombardment by monatomic and multiautomic Au ions and theoretical curves generated from Eq. (5) are shown in Figs. 3 and 4. The trends seen in Figs. 3 and 4 agree with those seen in the molecular ion yields measured by Benguerba *et al.*⁷ by subjecting solid organic films to bombardment from clusters of gold atoms.

From the curves presented in Figs. 1–4, it is clear that the probability of spike formation influences the secondary ion yield of large, intact molecules from the surface region of a condensed phase organic matrix when the latter is bombarded by heavy, monatomic ions such as Au^+ and Bi^+ . Further evidence for the influence of energy spikes on nonlinear sputtering effects produced by keV ions is contained in the yield data for the lighter, monatomic, primary ions Ga^+ and In^+ . Secondary ion yields of deprotonated dAMP molecules from the surface region of glycerol are shown versus nuclear stopping power and primary ion energy, respectively, in Figs. 5 and 6 for the primary ions Ga^+ , In^+ , and Bi^+ . Again the results of calculation with Eq. (5) are seen to agree satisfactorily with the experimental data. The fact that the fitted parameters have the same values for all of the theoret-

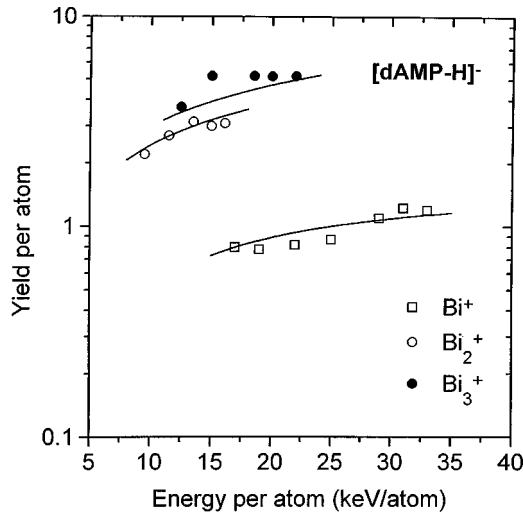


FIG. 2. Relative yield of deprotonated dAMP molecules per atom of a primary Bi_n ion ($n=1-3$) versus the impact energy per incident atom. Experimental data are from Ref. 35. Curves were computed with Eq. (5) using the same values for the adjustable parameters as given in Fig. 1.

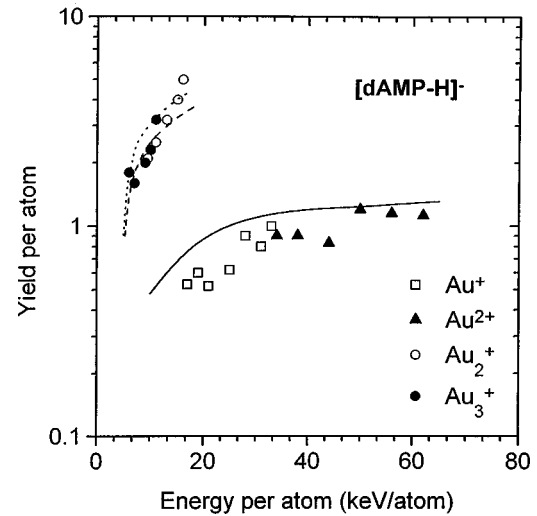


FIG. 4. Relative yield of deprotonated dAMP molecules per atom of a primary Au_n ion ($n=1-3$) versus the impact energy per incident atom. Experimental data are from Ref. 35. Curves were computed with Eq. (5) using the same values for the adjustable parameters as given in Fig. 1. Solid curve is for Au_1 , the dashed curve is for Au_2 , and the dotted curve is for Au_3 .

ical curves shown in the two figures supports the assumption that these parameters depend solely on the characteristics of the matrix and the secondary molecule.

Derivations based on the existing spike models²¹⁻²⁴ lead to expressions for secondary ion yield that depend only on some power of ϵ and predict, therefore, that secondary ion yield should mimic relative trends in stopping power. The experimental points plotted in Figs. 5 and 6 clearly do not lie on a single curve. Hence in this instance, stopping power alone does not account for the observed secondary molecular ion yields, a fact that fundamentally typifies nonlinear sputtering phenomena observed under keV-ion bombardment. The calculated nuclear stopping powers of the three non-

atomic primary ions Ga^+ , In^+ , and Bi^+ are shown in Fig. 7 as a function of the kinetic energy of the primary ions. From the figure, it can be seen that $\epsilon(\text{Bi})/\epsilon(\text{Ga})=1$ at $E_0 \approx 17$ keV. This being so, it is remarkable that at this impact energy the secondary molecular ion yield resulting from bombardment by Bi^+ is about one order of magnitude larger than that resulting from bombardment by Ga^+ (Fig. 6). Moreover, the trends of the Bi^+ and Ga^+ data plotted in Fig. 6 suggest that the yield for Bi^+ remains significantly higher than that for Ga^+ even at incident energies below 17 keV where, according to Fig. 7, $\epsilon(\text{Bi})/\epsilon(\text{Ga}) < 1$.

To gain a better understanding of how the relative yields from two bombarding species can behave oppositely to their

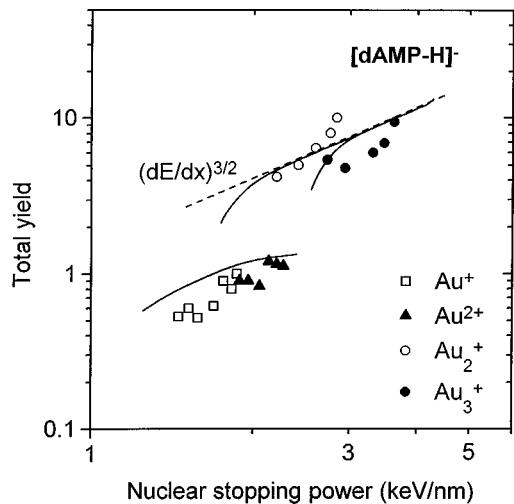


FIG. 3. Relative total yield of deprotonated dAMP molecules from the surface region of glycerol versus the stopping powers of Au_n ions ($n=1-3$). Experimental data are from Ref. 35. Dashed line represents $Y \propto (dE/dx)^{3/2}$. Solid curves were generated with Eq. (5) using the same values for the adjustable parameters as given in Fig. 1.

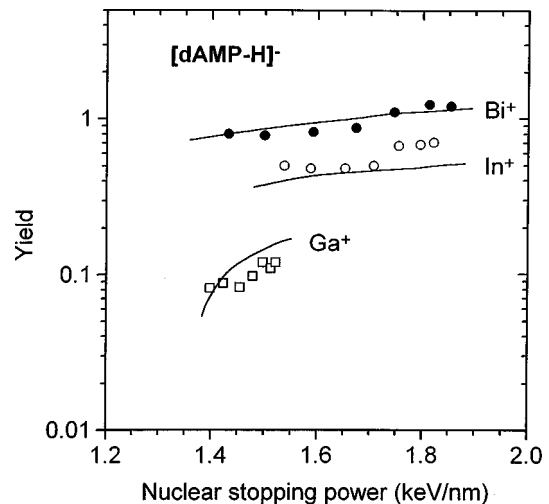


FIG. 5. Relative total yield of deprotonated dAMP molecules from the surface region of glycerol versus the stopping powers of Ga^+ , In^+ , and Bi^+ . Experimental data are from Ref. 35. Solid curves were generated with Eq. (5) using the same values for the adjustable parameters as given in Fig. 1.

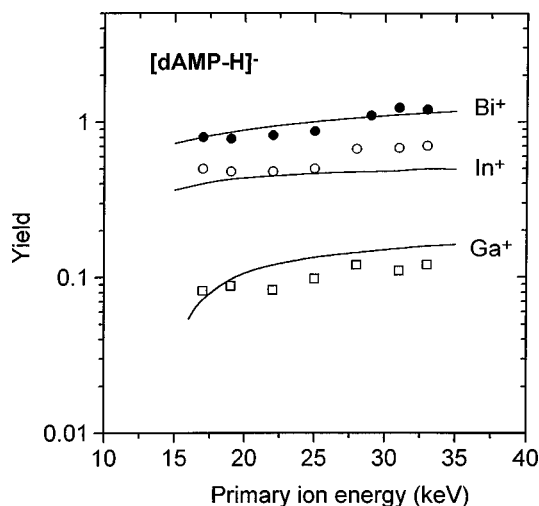


FIG. 6. Relative total yield of deprotonated dAMP molecules versus the impact energy of the primary ions Ga^+ , In^+ , and Bi^+ . Experimental data are from Ref. 35. Curves were computed with Eq. (5) using the same values for the adjustable parameters as given in Fig. 1.

relative energy losses in the target, it is useful to examine how the magnitude of the secondary ion yield predicted by Eq. (5) depends on the integral's lower limit. This behavior is governed by the probability of energy-loss straggling expressed in the distribution function $p(z) = \exp[-\alpha n \epsilon d(z + 1/z - 2)]$ found in the integrand of Eq. (5). The spread of this function about its maximum at $z = (E_c/n\epsilon d) = 1$ is determined by the characteristics of the bombarding species through the quantity $\alpha n \epsilon d$. For the range of primary ion impact energies under consideration in this paper, $\alpha n \epsilon d$ is greater than unity. Plots of $p(z)$ are shown in Fig. 8 for Ga^+ , Bi^+ , and Bi_2^+ particles incident on glycerol. The integral's lower limit $E_c/n\epsilon d$ exceeds 1 for bombardment of glycerol by 17 keV Ga^+ or Bi^+ (Fig. 8). It will be recalled from the statement immediately following Eq. (5) that $E_c/n\epsilon d$ is in-

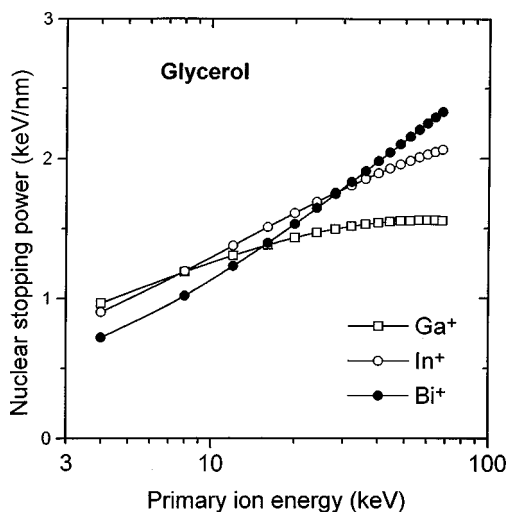


FIG. 7. Nuclear stopping powers of Ga^+ , In^+ , and Bi^+ in glycerol versus primary ion impact energy. The stopping power curves were calculated using Eq. (10) for the Kr-C potential (Ref. 39) and Bragg's law.

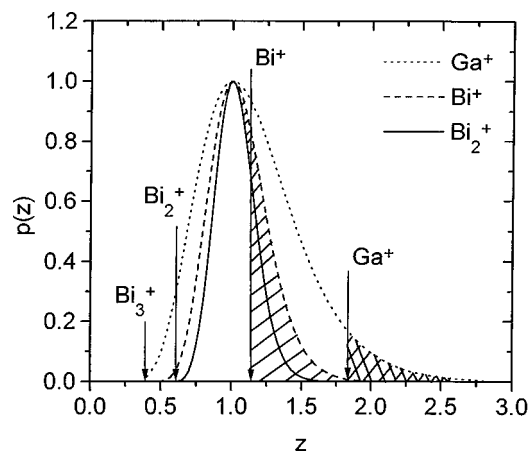


FIG. 8. Plots of $p(z) = \exp[-\alpha n \epsilon d(z + 1/z - 2)]$ versus z for 17 keV/atom Ga^+ , Bi^+ , and Bi_2^+ impacting on glycerol: $\alpha n \epsilon d = 4.7(\text{Ga}^+)$, $12.8(\text{Bi}^+)$, and $25.6(\text{Bi}_2^+)$. Arrows point to values on the abscissa corresponding to the lower limit of the integral in Eq. (5) for the indicated projectiles. For comparison, the integral's lower limit for 17 keV/atom Bi_3^+ is indicated on the abscissa, but the curve for this ion is not shown (it would be narrower than the curve for Bi_2^+). The magnitudes of the yields predicted by Eq. (5) for bombardment by Ga^+ and Bi^+ are proportional, respectively, to the area under the Ga^+ curve indicated with crosshatched lines and the area under the Bi^+ curve indicated with diagonal lines; these areas represent the probabilities respectively of a Ga^+ primary and a Bi^+ primary forming an energy spike.

versely proportional to the energy density $n\epsilon/\pi\bar{r}^2$ left in the wake of a primary particle. Inspection of Eqs. (8) and (9) quickly reveals that \bar{r}^2 is proportional to $(\gamma/4)^{2m} = [M_1 M_2 / (M_1 + M_2)^2]^{2m}$, which under the conditions being considered (viz. $M_1 \geq 70u$ and $M_2 = 6.6u$) reduces effectively to $\bar{r}^2 \propto (M_2/M_1)^{2m}$. Thus, for $m = 0.23$ (see caption for Fig. 1), $\bar{r}^2(\text{Ga})/\bar{r}^2(\text{Bi}) \approx (209/70)^{0.46} \approx 1.7$. Since $\epsilon(\text{Ga})/\epsilon(\text{Bi}) = 1$ at $E_0 \approx 17$ keV (Fig. 7), $[E_c/n\epsilon d(\text{Ga})]/[E_c/n\epsilon d(\text{Bi})] = [\bar{r}^2/\epsilon(\text{Ga})]/[\bar{r}^2/\epsilon(\text{Bi})] \approx 1.7$. In other words, a 17 keV Bi ion loses the same amount of energy as a 17 keV Ga ion over a given distance in glycerol, but the energy density generated along the Bi projectile's path is 1.7 times greater than that along the Ga projectile's. Therefore, the integral in Eq. (5) has a smaller lower limit for a Bi^+ impact than for a Ga^+ impact, which, as seen in Fig. 8, gives rise to a dramatic increase in the probability of spike formation and, therefore, the yield produced by Bi^+ over that produced by Ga^+ .

Multiatomic keV projectiles, such as Bi_2 and Bi_3 , raise the energy density along their paths through glycerol much more than monatomic species. The lower limit of the integral in Eq. (5), $E_c/n\epsilon d$, reflects this physical situation by becoming less than 1 (Fig. 8). Thus, the integral becomes weakly dependent on its lower limit and reduces to the form given by Eq. (6), which correctly predicts that the yields generated by multiatomic projectiles will for all practical purposes fall on a single energy-loss curve as is seen in Figs. 2 and 4.

The yield of the surfactant cations, HDP^+ , from glycerol was also reported by Yen and Barofsky.³⁵ They were able to extend their measurements of this secondary species, which is the principal counter ion to $[\text{dAMP-H}]^-$, into a lower

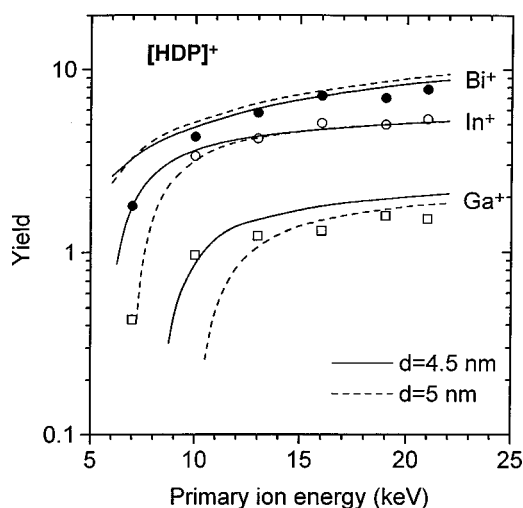


FIG. 9. Relative total yield of HDP^+ from the surface region of glycerol versus the primary ion's energy. Experimental data are from Ref. 35. Curves were computed with Eq. (5) using the same values for the adjustable parameters as given in Fig. 1 except for those of β and d .

range of impact energies (7–21 keV) than was possible for $[\text{dAMP-H}^-]$. The yield of HDP^+ versus primary ion energy is shown in Fig. 9. As in the case of $[\text{dAMP-H}^-]$ (Fig. 5), the experimental points produced by the monatomic primaries Ga^+ , In^+ , and Bi^+ fall on distinctly different curves. Figure 9 also shows the yield of HDP^+ predicted by Eq. (5). The calculated curves are, for the most part, in good agreement with the experimental points indicating that energy straggling plays basically the same role for the cation as for the anion. It is worth emphasizing that evaluation of Eq. (5) for HDP^+ only required that the values of the two parameters β and d be changed from those used for dAMP (see caption under Fig. 1).

It is also evident from Fig. 9 that, for incident energies less than about 10 keV, Eq. (5) underestimates the yield of HDP^+ secondaries; this discrepancy is especially pronounced in the case of Ga^+ , the lightest projectile. A similar disagreement was found to exist between the yields of positive molecular ions of alanine sputtered off aluminized Mylar substrates by keV-alkali ions¹⁴ and the yields calculated from the spike probability model.³³ These differences between experiment and theory can be explained in large part by examining how d , the parameter that describes the thickness of the zone where the spikes are initiated, depends on the kinetic energy of the primary ions. For values of d on the order of one or two mean interatomic spacings in a condensed phase, a primary ion can only unleash one or two nonoverlapping elastic collision cascades; therefore, the probability of spike formation is low. For values of d on the order of an incident ion's full range of penetration, the probability of forming spikes is also low unless the mean stopping power is quite high. Between these two extremes, there exists a d that maximizes the probability of spike formation. The calculated curves for $[\text{dAMP-H}^-]$ shown in Figs. 1–6 indicate that this optimal distance remains effectively constant over a broad range of primary ion energies. When, however, incident ion energies become comparable to E_c ,

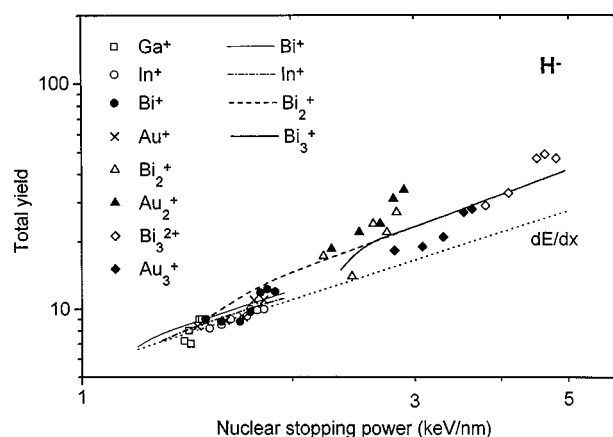


FIG. 10. Relative total yield of H^- from the surface region of glycerol versus the stopping powers of several monatomic and multiatomic primary ions. Experimental data are from Ref. 35. The curves for Bi^+ , In^+ , Bi_2^+ , and Bi_3^+ were computed with Eq. (5) using the same values for the adjustable parameters as given in Fig. 1. The dotted curve is $Y_{\text{linear}} \propto (dE/dx)$ (the absolute value of H^- yield cannot be calculated from cascade theory). The contribution to H^- yield resulting from the spike induced by an impacting Ga^+ is such a small percentage of that resulting from the linear cascade induced by the same particle that the curve for H^- yield calculated from Eq. (5) (not shown) nearly coincides with Y_{linear} . The curves for the H^- yields induced by the impact of Au_n^+ particles are not drawn because they are nearly indistinguishable from those shown for Bi_n^+ impacts.

energy deposition apparently becomes more efficient, and consequently, spikes are initiated in a narrower zone. Examination of the yield curves in Fig. 9, which were calculated for $d=4.5$ nm and $d=5.0$ nm, indicates that this circumstance arises as both incident energies become lower and projectiles become lighter. For example, the yield of HDP^+ induced by heavy Bi^+ impact is practically insensitive to the reduction in d from 5.0 to 4.5 nm, whereas the yields induced by Ga^+ and In^+ are clearly best fit by Eq. (5) when $d=4.5$ nm. It is remarkable that in the lower range of impact energies the yield induced by Bi^+ primaries remains about one order of magnitude larger than that induced by Ga^+ primaries (Fig. 9) despite the fact that the stopping power of a Bi^+ in this range is less than that of a Ga^+ (Fig. 7).

Linear cascades contribute negligibly to the desorption of intact organic molecules but significantly to the secondary emission of individual atoms. Therefore, the availability of experimental data for the emission of hydride ions³⁵ provides an opportunity to apply the spike probability model to a situation in which linear cascades should be taken into account. The experimental yield of H^- is shown in Fig. 10 plotted against the nuclear stopping powers of a variety of primary ions. In addition, Fig. 10 shows curves generated with Eq. (5) for monatomic and multiatomic bombardment and, for comparison, a curve predicted from Sigmund's linear cascade theory.¹ It is noteworthy that with the exception of the value of β , which is specific to a given secondary species, the values of the parameters used to calculate the curves for H^- yield in Fig. 10 were the same as those given in Fig. 1.

In contrast to the desorption of intact organic molecules, the yields of H^- for all four of the atomic projectiles Ga^+ ,

In^+ , Au^+ , and Bi^+ lie, within experimental error, on the single straight line $Y_{\text{linear}} \propto (dE/dx)$ predicted from linear cascade theory. The curves for monatomic projectiles generated from the spike probability model, i.e., Eq. (5), all lie slightly above Y_{linear} , but they are still within the margins of the data's experimental error. Thus, if it is assumed that the yields of a secondary ion due respectively to linear cascades and spikes are additive, i.e., $Y_{\text{observed}} = Y_{\text{linear}} + Y_{\text{spike}}$, it is evident from Fig. 10 that under monatomic ion bombardment spike effects do not play a significant role in the secondary emission of H^- .

The experimental yields of H^- resulting from multiatomic bombardment are more scattered than those from monatomic bombardment; nevertheless with the exception of a single point for Bi_2^+ , they all obviously lie well above Y_{linear} . In contrast to the linear cascade model, the spike probability model produces different curves for the yields of H^- due to monatomic ion bombardment and those due to multiatomic ion bombardment. Similarly, Stenum *et al.*⁴⁴ found in their analysis of the experimental results reported by Oliva-Florio *et al.*⁶ that the yields produced by monatomic and multiatomic projectiles fell upon separate curves; subsequent analysis of this same data within the framework of the spike probability model disclosed the same feature.³⁴ The curves produced by Eq. (5) for multiatomic projectiles reflects reasonably well the enhancement in the measured yields despite the experimental scatter. This, of course, suggests that contributions from Y_{spike} are much more pronounced for multiatomic ion bombardment than for monatomic ion bombardment.

C. Possibility for future experiments

The spike probability model predicts that the nonlinear increase in the yield of intact molecules due to multiatomic ion bombardment should become more pronounced for projectiles composed of light elements. This outcome of the model is most conveniently expressed in terms of the enhancement factor introduced by Benguerba *et al.*⁷

$$t_{mn} = \frac{Y_m/m}{Y_n/n} \quad (m > n), \quad (11)$$

where Y_m and Y_n are the secondary ion yields due to equi-velocity projectiles having m and n atoms of the same element, respectively. In the absence of nonlinear phenomena, the secondary ion yield depends linearly on stopping power, i.e., $Y_n \propto n(dE/dx)$, and consequently, the enhancement factor $t_{mn} = 1$. For the earlier spike models,¹⁹⁻²³ in which $Y_n \propto n^\nu(dE/dx)^\nu$ ($\nu > 1$), Eq. (11) reduces to

$$t_{mn} = \left(\frac{m}{n}\right)^{\nu-1}. \quad (12)$$

However, the spike probability model under discussion in the present paper leads to this simple relation only when the stopping power of the primary ion is high enough for Eq. (6) to prevail. When the stopping power of the primary ion is low and the expression for Y_{spike} is given by Eq. (7), the magnitude of the enhancement factor becomes much greater than predicted by Eq. (12).

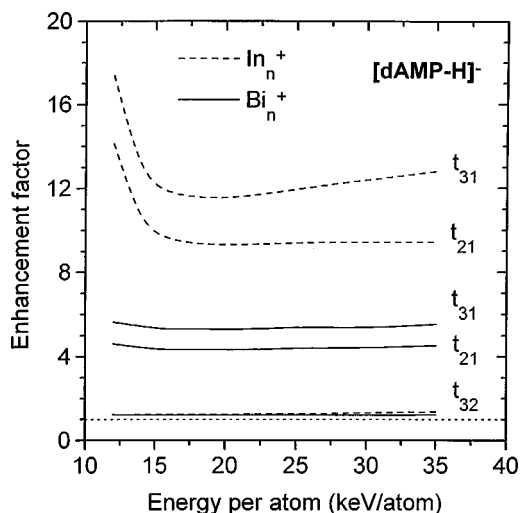


FIG. 11. Enhancement factors t_{mn} ($m=2$ and 3 , $n=1$ and 2) for $[\text{dAMP-H}]^-$ bombarded by In_n and Bi_n as a function of the kinetic energy per atom of the incident particle. No enhancement would be expected in the absence of nonlinear phenomena, this is represented by $t_{mn} = 1$ (dotted line).

Plots of various enhancement factors versus primary ion energy per atom, which were calculated using Eqs. (6) and (12) for deprotonated dAMP sputtered from glycerol by In_n and by Bi_n , are displayed in Fig. 11. For the heavier Bi_n projectiles, $t_{21} \approx 4.5$ and $t_{31} \approx 5.5$; in light of the data shown in Fig. 2, these values are in good agreement with experiment. By comparison, Eq. (12) with $\nu = \frac{3}{2}$ gives $t_{21} \approx 1.4$ and $t_{31} \approx 1.7$, values that are less than one third of those predicted by the spike probability model. These contrasting results emphasize the significance of taking into account the probability of spike formation, which is relatively high when glycerol is bombarded by multiatomic projectiles. For the lighter In_n projectiles, the difference between the yield enhancement factors calculated from Eq. (5) and those calculated from Eq. (12) are even more pronounced than in the case of Bi_n primary ions (Fig. 11); this is especially so for impact energies below 15 keV. Comparing two- and three-atom projectiles, the yield enhancement factors obtained from Eq. (5) turn out to be nearly the same for both In_n and Bi_n primary ions ($t_{32} \approx 1.24$) as well as to be very close to the value obtained from Eq. (12) [$t_{32} = (\frac{3}{2})^{0.5} \approx 1.22$]. Measurements of enhancement factors for much lighter projectiles, e.g., Ga or Al, would make it possible to test the spike probability model in a stopping power domain heretofore unexplored.

Nonlinear sputtering yields were not observed in a recent study carried out with coronene, coronene dimers, C_{37} , C_{60} , and C_{70} as projectiles.¹⁸ This experimental result would appear to contradict our prediction that bombardment with clusters of light elements should produce large enhancements in molecular yield. However, the incident energy per atom of the big clusters used in these experiments was just a few hundred eV, considerably below that which is necessary to create spikes as discussed in this paper. In such cases, it seems more likely that the sputtering yield depends on the projectile's total kinetic energy rather than its stopping power. If one assumes that the sputtered particles originate from a crater whose volume is proportional to the total ki-

netic energy of the incident cluster as recently proposed by Zubarev *et al.*,⁴⁵ one finds that the emission yield per unit mass of the incident projectile is, in fact, proportional to the energy per unit mass of the incident projectile as observed by Boussofiane-Baudin *et al.*¹⁸

VI. CONCLUSIONS

The nonlinear sputtering effects observed when liquid organics are bombarded by atomic and multiatomic keV ions are described well when energy-loss straggling in the transfer of primary ion energy to the target is used as a basis for calculating the probability of forming energy spikes. It is noteworthy that this spike probability model accounts for experimental yields in several cases where treatments based solely on mean stopping power are found deficient. Specifically, the model's more complete description seems to be required when, as in the case of intact molecules sputtered from condensed organic phases, spike phenomena predomi-

nate. In the case of light projectiles, it would be worthwhile to calculate enhancement factors and use the results as predictions to guide further experimentation. Such experiments would have the added benefit of providing information about the exponent ν that governs the secondary ion yield's nonlinear dependence on the stopping power in Eq. (5).

ACKNOWLEDGMENTS

Primary support for I.S.B. was provided by the Swedish Natural Sciences Research Council (NFR) and the Ångström and Cluster Consortia; additional support for finishing the work was given by the Danish Research Academy and the Danish Natural Science Research Council. Support for D.F.B. was provided by Grant No. ES00210 from the U.S. National Institute of Environmental Health Sciences. The authors thank P. Sigmund and R.E. Johnson for helpful discussions.

-
- ¹P. Sigmund, *Phys. Rev.* **184**, 383 (1969).
²H. H. Andersen and H. L. Bay, in *Sputtering by Particle Bombardment I*, edited by R. Behrisch (Springer Verlag, Berlin, 1981), p. 145.
³H. H. Andersen and H. L. Bay, *Radiat. Eff.* **19**, 139 (1973).
⁴H. H. Andersen and H. L. Bay, *J. Appl. Phys.* **45**, 953 (1974).
⁵S. S. Johar and D. A. Thompson, *Surf. Sci.* **90**, 319 (1979).
⁶A. R. Oliva-Florio, E. V. Alonso, R. A. Baragiola, J. Ferron, and M. M. Jakas, *Radiat. Eff.* **50**, 3 (1979).
⁷M. Benguerba, A. Brurielle, S. Della-Negra, J. Depauw, H. Joret, Y. Le Beyec, G. Blain, A. Schweikert, G. Ben Assayag, and P. Sudraud, *Nucl. Instrum. Methods Phys. Res. B* **62**, 8 (1991).
⁸K. B. Ray, M. A. Park, and E. A. Schweikert, *Nucl. Instrum. Methods Phys. Res. B* **82**, 317 (1993).
⁹H. H. Andersen, *K. Dan. Vidensk. Selsk. Mat. Fys. Medd.* **43**, 127 (1993).
¹⁰I. Katakuse, T. Ishihara, Y. Fujita, T. Matsuo, T. Sakurai, and H. Matsuda, *Int. J. Mass Spectrom. Ion Processes* **67**, 229 (1985).
¹¹N. K. Dzhemilev, S. V. Verkhoturov, and V. Veriovin, *Nucl. Instrum. Methods Phys. Res. B* **51**, 219 (1990).
¹²A. Wucher, M. Wahl, and H. Oechsner, *Nucl. Instrum. Methods Phys. Res. B* **82**, 337 (1993).
¹³S. R. Coon, W. F. Calaway, M. J. Pellin, and J. M. White, *Surf. Sci.* **298**, 161 (1993).
¹⁴K. G. Standing, B. Chait, W. Ens, G. McIntosh, and R. Beavis, *Nucl. Instrum. Methods Phys. Res.* **198**, 33 (1982).
¹⁵W. Ens, B. U. R. Sundqvist, P. Håkansson, D. Fenyö, A. Hedin, and G. Jonsson, *J. Phys. (Paris)* **50**, 9 (1989).
¹⁶S. Della-Negra, J. Depauw, H. Joret, and Y. Le Beyec, *J. Phys. (Paris)* **50**, 63 (1989).
¹⁷R. Galera, J.-C. Blais, and G. Bolbach, *Int. J. Mass Spectrom. Ion Processes* **107**, 531 (1991).
¹⁸K. Boussofiane-Baudin, G. Bolbach, A. Brunelle, S. Della-Negra, P. Håkansson, and Y. Le Beyec, *Nucl. Instrum. Methods Phys. Res. B* **88**, 160 (1994).
¹⁹P. Sigmund, *Appl. Phys. Lett.* **25**, 169 (1974).
²⁰P. Sigmund, *Appl. Phys. Lett.* **27**, 52 (1975).
²¹G. H. Vineyard, *Radiat. Eff.* **29**, 245 (1976).
²²R. E. Johnson and E. Evatt, *Radiat. Eff.* **52**, 187 (1980).
²³P. Sigmund and C. Claussen, *J. Appl. Phys.* **52**, 990 (1981).
²⁴Y. Kitazoe and Y. Yamamura, *Surf. Sci.* **111**, 381 (1981).
²⁵W. Ens, *K. Dan. Vidensk. Selsk. Mat. Fys. Medd.* **43**, 155 (1993).
²⁶K. L. Merkle and W. Jäger, *Philos. Mag. A* **44**, 741 (1981).
²⁷M. H. Shapiro and T. A. Tombrello, *Nucl. Instrum. Methods Phys. Res. B* **48**, 557 (1990).
²⁸H. M. Urbassek and K. T. Waldeer, *Phys. Rev. Lett.* **67**, 105 (1991).
²⁹K. T. Waldeer and H. M. Urbassek, *Nucl. Instrum. Methods Phys. Res. B* **73**, 14 (1993).
³⁰Q. Yang, T. Li, B. V. King, and R. J. MacDonald, *Phys. Rev. B* **53**, 3032 (1996).
³¹U. Conrad and H. M. Urbassek, *Nucl. Instrum. Methods Phys. Res. B* **48**, 399 (1990).
³²J. E. Westmoreland and P. Sigmund, *Radiat. Eff.* **6**, 187 (1970).
³³I. S. Bitensky, *Nucl. Instrum. Methods Phys. Res. B* **83**, 110 (1993).
³⁴I. S. Bitensky, *Nucl. Instrum. Methods Phys. Res. B* **88**, 69 (1994).
³⁵T. Y. Yen and D. F. Barofsky, *Nucl. Instrum. Methods Phys. Res. B* (to be published).
³⁶J. Lindhard and V. Nielsen, *K. Dan. Vidensk. Selsk. Mat. Fys. Medd.* **38**, 9 (1971).
³⁷K. B. Winterbon, P. Sigmund, and J. B. Sanders, *K. Dan. Vidensk. Selsk. Mat. Fys. Medd.* **38**, 14 (1970).
³⁸D. Brandl, C. Schoppmann, R. Schmidt, B. Nees, A. Ostrowski, and H. Voit, *Phys. Rev. B* **43**, 5253 (1991).
³⁹W. D. Wilson, L. G. Haggmark, and J. P. Biersack, *Phys. Rev. B* **15**, 2458 (1977).
⁴⁰V. I. Shulga and P. Sigmund, *Nucl. Instrum. Methods Phys. Res. B* **47**, 236 (1990).
⁴¹L. F. Jiang, T. Y. Yen, and D. F. Barofsky, *Proceedings of the 37th ASMS Conference on Mass Spectrometry and Allied Topics* (American Society for Mass Spectrometry, Miami Beach, 1989), p. 1071.
⁴²D. F. Barofsky, L. F. Jiang, and T. Y. Yen, in *Ion Formation from Organic Solids (IFOS V)*, edited by A. Hedin, B. U. R. Sund-

- qvist, and A. Benninghoven (Wiley, Chichester, England, 1990), p. 87.
- ⁴³W. V. Ligon and S. B. Dorn, *Fresenius J. Anal. Chem.* **325**, 655 (1986).
- ⁴⁴B. Stenum, O. Ellegaard, J. Schou, H. Sørensen, and R. Pedrys, *Nucl. Instrum. Methods Phys. Res. B* **58**, 399 (1991).
- ⁴⁵R. A. Zubarev, I. S. Bitensky, P. A. Demirev, and B. U. R. Sundqvist, *Nucl. Instrum. Methods Phys. Res. B* **88**, 143 (1994).